APPLIED GEOPHYSICS, Vol.7, No.2 (June 2010), P. 174 - 184, 11 Figures.
DOI: 10.1007/s11770-010-0242-9

The Chebyshev spectral element method using staggered predictor and corrector for elastic wave simulations*

Che Cheng-Xuan[1], Wang Xiu-Ming[1], and Lin Wei-Jun[1]

Abstract: Based on strong and weak forms of elastic wave equations, a Chebyshev spectral element method (SEM) using the Galerkin variational principle is developed by discretizing the wave equation in the spatial and time domains and introducing the preconditioned conjugate gradient (PCG)-element by element (EBE) method in the spatial domain and the staggered predictor/corrector method in the time domain. The accuracy of our proposed method is verified by comparing it with a finite-difference method (FDM) for a homogeneous solid medium and a double layered solid medium with an inclined interface. The modeling results using the two methods are in good agreement with each other. Meanwhile, to show the algorithm capability, the suggested method is used to simulate the wave propagation in a layered medium with a topographic traction free surface. By introducing the EBE algorithm with an optimized tensor product technique, the proposed SEM is especially suitable for numerical simulation of wave propagations in complex models with irregularly free surfaces at a fast convergence rate, while keeping the advantage of the finite element method.
Keywords: Chebyshev spectral element, element by element, predictor/corrector algorithm

Introduction

In acoustic or seismic exploration, propagation characteristics of seismic waves in various complex media are required in order to acquire, process, and interpret seismic data and to use seismic data to invert formation properties. Numerical simulation is an efficient way to realize this goal. Therefore, considerable efforts are made to solve elastic wave equations and to simulate elastic wave propagation under various complex geologic conditions. For seeking a more efficient numerical method with high computation accuracy for simulating elastic wave propagation in complex geologic structures, many kinds of numerical modeling methods have been developed. However, for a given problem, a superior algorithm for general modeling cases is difficult to find and a specific algorithm is always chosen according to the specific situation because of the complexity of the problems researched.

Finite difference methods (FDM), finite element methods (FEM), and pseudo-spectral methods (PSM) are widely used in elastic wave modeling at present.

As a forward simulation method used most commonly, the FDM uses a difference operator instead of a differential operator in space and time and approximates the solution of the differential equation by solving the difference equation. Alterman and Loewenthal (1970) first applied this method to numerical simulation of the elastic wave equation. Later the accuracy of the FDM was studied by Alford et al. (1974). Since it is efficient and easy to implement, the FDM has been widely used

Manuscript received by the Editor November 24, 2009; revised manuscript received March 26, 2010.
*This work is supported by the National Natural Science Foundation of China (Grant No. 40774099, 10874202) and the National High Technology Research and Development Program of China (Grant No. 2008AA06Z205).
1. State Key Laboratory of Acoustics, Institute of Acoustics, Chinese Academy of Sciences, Beijing, 100190, China.

in seismic numerical simulation. However, this method requires enough mesh grids in a single wavelength to achieve an expected accuracy and it will not ensure the simulated accuracy or may even not work when dealing with steep topography and complex geologic configurati ons.

The FEM is another efficient forward simulation method and it is a significant breakthrough in the numerical analysis field. However, the FEM is not well used in large scale elastic wave simulation fields due to its larger memory requirements, time-consumption, and the lower computation efficiency. In addition, the low-order FEM has poor propagation characteristics which bring about strong dispersion errors, while conventional high-order FEM unfortunately generates spurious waves (Komatitsch and Vilotte., 1998).

The PSM was proposed by Gazdag (1981) and Kosloff and Baysal (1982). It only performs differential arithmetic operations in time and avoids differential arithmetic operations in space by performing the partial differential operations on spatial coordinates to implement the Fast Fourier Transform (FFT). Theoretically, the PSM has high accuracy and it can achieve machine precision by using even two mesh grids per wave length. However, performing forward and inverse FFTs repeatedly brings expensive computations. Similar to the FDM, the PSM can not deal with a topographic traction free surface and complex geologic configurations directly. Recently, its high accuracy is demurred and an improved technique is proposed (Wang et al., 2006).

The spectral element method (SEM), combining FEM with PSM, is learned from the fluid dynamics field. It has the flexibility of the FEM when handling boundaries and the fast convergence of the PSM. Compared with the FEM, the computation is greatly reduced and the computation accuracy is improved by introducing the element by element (EBE) technique to the SEM. The SEM was originally proposed by Patera (1984) for fluid dynamics. Seriani et al. (1992), Seriani and Priolo (1994), Seriani (1997, 1998) introduced the SEM for solving elastic wave equations and the related research work has been extended greatly by other researchers (Komatitsch et al., 1999, 2000a, 2000b, and 2002). The basic idea of the SEM is: first decompose the computation domain into many sub-domains with nodes and vertexes, then express the approximate solution as a truncated expansion of an orthogonal polynomial, and finally acquire the global approximate solution by solving the variational formulations of the orthogonal problem with a Galerkin approach.

In this paper, based on previous work (Lin et al., 2006; Wang et al., 2007), the fundamental principles of the Chebyshev SEM are summarized and the Chebyshev SEM algorithm for elastic wave modeling is achieved. Furthermore, the method is improved by introducing the preconditioned conjugate gradient (PCG)-element by element (EBE) method in the spatial domain and the staggered predictor/corrector method for time iterations. The modeling results of the SEM are compared with the FDM for a homogeneous medium and a medium with an inclined interface. In addition, the elastic wave propagation in a layered medium with a topographic traction-free surface is simulated using the proposed SEM and the generated waves are described and analyzed.

Principles of the Chebyshev SEM

The elastic wave equation and its weak form

Consider an elastic wave equation in two dimensions, let $\Omega \subset \mathbf{R}^{n_2}$ be an open set with piecewise smooth boundary Γ. We assume that Γ admits the decomposition $\Gamma = \overline{\Gamma_{\mathrm{gi}} + \Gamma_{\mathrm{hi}}}$, where $\Gamma_{\mathrm{gi}} \cap \Gamma_{\mathrm{hi}} = \varnothing$. Thus, given $t \in [0, \mathrm{T}]$, the strong form of the elastic wave equation with the boundary-value problem can be stated as follows (Hughes, 1987):

$$\begin{cases} \rho u_{i,tt} = \sigma_{ij,j} + f_i, & \Omega \times (0,\mathrm{T}) \\ u_i = g_i, & \Gamma_{gi} \times (0,\mathrm{T}) \\ \sigma_{ij} n_j = h_i, & \Gamma_{hi} \times (0,\mathrm{T}), \\ u_i(\vec{x},0) = u_{0i}(\vec{x}), & \vec{x} \in \Omega \\ u_{i,t}(\vec{x},t) = \dot{u}_{0i}(\vec{x}), & \vec{x} \in \Omega \end{cases} \tag{1}$$

where u_i is the displacement vector component in the i direction; σ_{ij} is the stress tensor, and $\sigma_{ij} = c_{ijkl} u_{k,l}$, with c_{ijkl} being the elastic tensor; Γ_{gi} and Γ_{hi} are displacement and stress boundaries, respectively; g_i and h_i are called the prescribed boundary displacements and tractions, respectively; $u_{0i}(\vec{x})$ and $\dot{u}_{0i}(\vec{x})$ are initial displacements and velocities, respectively.

The corresponding weak formulation is:

$$\begin{cases} (\mathbf{w}, \rho \ddot{\mathbf{u}}) + a(\mathbf{w}, \mathbf{u}) = (\mathbf{w}, \mathbf{f}) + (\mathbf{w}, \mathbf{h})_{\Gamma} \\ (\mathbf{w}, \rho \mathbf{u}(0)) = (\mathbf{w}, \rho \mathbf{u}_0), \\ (\mathbf{w}, \rho \dot{\mathbf{u}}(0)) = (\mathbf{w}, \rho \dot{\mathbf{u}}_0) \end{cases} \tag{2}$$

where $\mathbf{u}(t)\in\delta$ is a trial function; δ denotes a trial solution space, with members satisfying the displacement boundary condition and has a square-integrable first order derivative; $\mathbf{w}\in\nu$ is the test function with ν denoting a test solution space, also with members satisfying the zero displacement boundary conditions and a square-integrable first order derivative. The inner product in equation (2) can be stated as:

$$(\mathbf{w},\rho\ddot{\mathbf{u}})=\frac{\mathrm{d}^2}{\mathrm{d}t^2}\int_\Omega \rho w_i u_i \,\mathrm{d}\Omega, \tag{3}$$

$$a(\mathbf{w},\mathbf{u})=\int_\Omega w_{(i,j)}c_{ijkl}u_{(k,l)}\,\mathrm{d}\Omega, \tag{4}$$

$$(\mathbf{w},\mathbf{f})=\int_\Omega w_i f_i \,\mathrm{d}\Omega,\triangleright, \tag{5}$$

$$(\mathbf{w},\mathbf{h})_\Gamma=\sum_{i=1}^{n_{sd}}\left(\int_{\Gamma_{hi}} w_i h_i \,\mathrm{d}\Gamma\right), \tag{6}$$

where $\mathbf{w}=w_i\mathbf{e}_i$ with $\mathbf{e}_i$ the unit vector and i and j are the symmetric parts of the tensor.

Spatial discretization

The physical domain Ω is discretized into n_e non-overlapping quadrilateral elements Ω_e, $\Omega=\cup\Omega_e$. On each element, the solution is approximated by the Chebyshev interpolation function defined at the collocation points. Figure 1 shows the arrangement of reference nodes based on the Chebyshev polynomials, where the nodes are called Chebyshev-Gauss-Labatto points in each dimension, with the value $x_i=\cos[\pi i/(N-1)]$, for $i=0$, N-1, and N is the number of nodes in each dimension (Canuto et al., 1988).

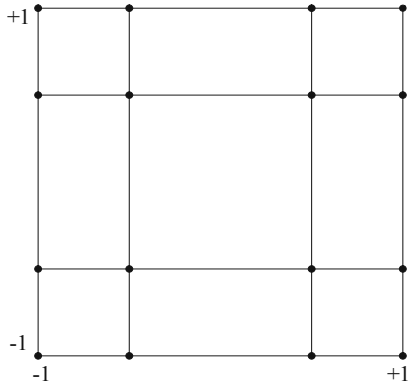

Fig. 1 Arrangement of nodes and vertexes.

Let δ^h and ν^h denote the trial solution and the test solution spaces defined on the element, respectively, and also $\delta^h\subset\delta$ and $\nu^h\subset\nu$. We assume that all members $\mathbf{w}^h\in\nu$ satisfy $w_i=0$ on Γ_{gi} and that each member of δ^h admits the representation $\mathbf{u}^h=\mathbf{v}^h+\mathbf{g}^h$, where $\mathbf{v}^h\in\nu^h$ and $\mathbf{g}^h$ results in satisfaction of the boundary condition $u_i=g_i$ on Γ_{gi}

Then, the discrete Galerkin formulation can be written as:

$$\begin{cases}(\mathbf{w}^h,\rho\ddot{\mathbf{v}}^h)+a(\mathbf{w}^h,\rho\mathbf{v}^h)=(\mathbf{w}^h,\mathbf{f})\\ +(\mathbf{w}^h,\mathbf{h})_\Gamma-(\mathbf{w}^h,\rho\ddot{\mathbf{g}}^h)-a(\mathbf{w}^h,\mathbf{g}^h)\\ (\mathbf{w}^h,\rho\mathbf{v}^h(0))=(\mathbf{w}^h,\rho\mathbf{u}_0)-(\mathbf{w}^h,\rho\mathbf{g}^h(0))\\ (\mathbf{w}^h,\rho\dot{\mathbf{v}}^h(0))=(\mathbf{w}^h,\rho\dot{\mathbf{u}}_0)-(\mathbf{w}^h,\rho\dot{\mathbf{g}}^h(0))\end{cases}, \tag{7}$$

The expressions of $\mathbf{w}^h$, $\mathbf{v}^h$ and $\mathbf{g}^h$ are shown as:

$$\mathbf{w}^h=w_i^h\mathbf{e}_i,\quad w_i^h(\vec{x},t)=\sum_{A\in\eta-\eta_{gi}}N_A(\vec{x})c_{iA}(t), \tag{8}$$

$$\mathbf{v}^h=v_i^h\mathbf{e}_i,\quad v_i^h(\vec{x},t)=\sum_{A\in\eta-\eta_{gi}}N_A(\vec{x})d_{iA}(t), \tag{9}$$

$$\mathbf{g}^h=g_i^h\mathbf{e}_i,\quad g_i^h(\vec{x},t)=\sum_{A\in\eta_{gi}}N_A(\vec{x})g_{iA}(t), \tag{10}$$

where A is the node on element Ω^{n2}; η, $\eta_{gi}\in\{1,2,\ldots,N\}$ is the node number, and $u_i^h=g_i$ holds for η_{gi}; and $\mathbf{e}_i$ is the unit vector.

Based on this analysis, a second-order semi-discretization ordinary differential equation with respect to time can be expressed as follows:

$$\begin{cases}\mathbf{M}\ddot{\mathbf{U}}+\mathbf{K}\mathbf{U}=\mathbf{F}\\ \mathbf{U}(0)=\mathbf{U}_0\\ \dot{\mathbf{U}}(0)=\dot{\mathbf{U}}_0\end{cases}, \tag{11}$$

where $\mathbf{M}$ is the global mass matrix; $\mathbf{K}$ is the global stiffness matrix; $\mathbf{F}$ is the body force or gravity, and $\mathbf{U}$ is the displacement vector.

Time discretization

In order to solve the system of semi-discretization equations in equation (11), integration is needed over the time interval [0,T] and this may be done by discretizing the time domain. In this paper, an α method by Hilber et al. (1977) is adopted to perform this operation by introducing three control variables α, β, and γ. Through discretizations, the equation $\mathbf{M}\ddot{\mathbf{U}}+\mathbf{K}\mathbf{U}=\mathbf{F}$ can be expressed as:

$$\mathbf{M}\mathbf{a}_{n+1}+(1+\alpha)\mathbf{C}\mathbf{v}_{n+1}-\alpha\mathbf{C}\mathbf{v}_n+(1+\alpha)\mathbf{K}\mathbf{U}_{n+1}-\alpha\mathbf{K}\mathbf{U}_n=\mathbf{F}(t_{n+\alpha}), \tag{12}$$

$$\mathbf{U}_{n+1} = \tilde{\mathbf{U}}_{n+1} + (1+\alpha)\beta\Delta t^2 \mathbf{a}_{n+1}, \tag{13}$$

$$\mathbf{v}_{n+1} = \tilde{\mathbf{v}}_{n+1} + (1+\alpha)\gamma\Delta t \mathbf{a}_{n+1}, \tag{14}$$

$$\tilde{\mathbf{U}}_{n+1} = \mathbf{U}_n + (1+\alpha)\Delta t \mathbf{v}_n + \frac{\Delta t^2}{2}(1+\alpha) \times (1-2\beta)\mathbf{a}_n, \tag{15}$$

$$\tilde{\mathbf{v}}_{n+1} = \mathbf{v}_n + \Delta t(1+\alpha)(1-\gamma)\mathbf{a}_n, \tag{16}$$

$$t_{n+\alpha} = (1+\alpha)t_{n+1} - \alpha t_n = t_{n+1} + \alpha\Delta t, \tag{17}$$

$$\begin{cases} \alpha \in [-1/3, 0] \\ \beta = (1-\alpha)^2/4, \\ \gamma = (1-2\alpha)/2 \end{cases} \tag{18}$$

Based on equations (13) to (18), equation (12) can be rewritten as:

$$\mathbf{M}^* \mathbf{a}_{n+1} = \mathbf{F}^*, \tag{19}$$

where

$$\mathbf{M}^* = \mathbf{M} + \gamma(1+\alpha)^2 \Delta t \mathbf{C} + \beta(1+\alpha)^2 \Delta t^2 \mathbf{K},$$

and

$$\mathbf{F}^* = \mathbf{F}(t_{n+\alpha}) - \mathbf{C}\tilde{\mathbf{v}}_{n+1} - \mathbf{K}\tilde{\mathbf{U}}_{n+1}.$$

Element by element technique

The EBE technique was originally used for heat conduction problems (Hughes et al., 1983a) and for solid and structure mechanics (Hughes et al., 1983b). Seriani (1997) was the first to introduce this method into the SEM for solving elastic wave equations. Its basic idea is to decompose the global scale computations into many unattached local scale computations without forming the global stiffness matrix.

Consider a system of equations $\mathbf{Ax}=\mathbf{b}$, where $\mathbf{A}=(a_{ij}) \in \mathbf{R}^{n\times n}$ is an n-order symmetric positive definite matrix, $\mathbf{x}=(x_1,\ldots,x_n)^{\mathrm{T}}$ and $\mathbf{b}=(b_1,\ldots,b_n)^{\mathrm{T}}$. $\mathbf{A}$ and $\mathbf{x}$ can be formed by combining $\mathbf{A}_e$ and $\mathbf{x}_e$ according to the element view, namely:

$$\mathbf{b} = \mathbf{A}\cdot\mathbf{x} = \sum_e (\mathbf{A}_e \cdot \mathbf{x}_e), \tag{20}$$

where $\mathbf{A}_e$ and $\mathbf{x}_e$ are the element matrix and vector that compose the global matrix and vector, respectively. $\mathbf{A}_e$ and $\mathbf{x}_e$ are only related with the element e and there is no need to compute the values of $\mathbf{A}_e \cdot \mathbf{x}_e$. We can just compute the value of $\mathbf{b}_e=\mathbf{A}_e \cdot \mathbf{x}_e$, with $\mathbf{A}_e$ and $\mathbf{x}_e$ being the local element matrix and vector, respectively, and then add $\mathbf{b}^e$ to $\mathbf{b}$. Thus, only the local element matrix is stored and the global matrix is not really used in getting the global vector, which reduces the computation costs and memory requirements.

Staggered predictor and corrector algorithm

In order to solve equation (19), the staggered predictor/corrector algorithm (Hughes, 1987) with flexible time step length is introduced into the traditional SEM. The detailed process is:

1. $n=0$ (index of time iteration),

$$\tilde{\mathbf{U}}_n = \mathbf{U}_n + (1+\alpha)\Delta t \mathbf{v}_n + (1+\alpha)(1-2\beta)\Delta t^2 \mathbf{a}_n/2.$$

2. $\tilde{\mathbf{v}}_n = \mathbf{v}_n + (1+\alpha)(1-\gamma)\Delta t \mathbf{a}_n$,

$\tilde{\mathbf{a}}^1 = 0$.

3. Do loop for i, solve

$$\mathbf{M}^* \Delta \mathbf{a}^{(i)} = \Delta \mathbf{F}^{*(i)},$$

$$\tilde{\mathbf{U}}^{(i+1)} = \tilde{\mathbf{U}}^{(i)} + (1+\alpha)\beta\Delta t^2 \Delta \mathbf{a}^{(i)},$$

$$\mathbf{v}^{(i+1)} = \tilde{\mathbf{v}}^{(i)} + (1+\alpha)\gamma\Delta t \Delta \mathbf{a}^{(i)},$$

$$\tilde{\mathbf{a}}^{(i+1)} = \tilde{\mathbf{a}}^{(i)} + \Delta \mathbf{a}^{(i)},\ \mathbf{a}_{n+1} = \tilde{\mathbf{a}}^{(i+1)},$$

4. End loop, $\mathbf{v}_{n+1} = (\tilde{\mathbf{v}}_{n+1} - \mathbf{v}_n)/(1+\alpha) + \mathbf{v}_n$,

$$\mathbf{U}_{n+1} = (\tilde{\mathbf{U}}_{n+1} - \mathbf{U}_n)/(1+\alpha) + \mathbf{U}_n.$$

If it is not the end of time iteration, $n=n+1$, and then continue the next iteration, or else, stop.

EBE iteration algorithm

In the process of the time iteration, the major segment is to solve the equation $\mathbf{M}^*\mathbf{a}_{n+1}=\mathbf{F}^*$, which is written as $\mathbf{SX}=\mathbf{B}$ for convenience. The combination of the EBE algorithm and the preconditioned conjugate gradient (PCG) is used to solve the previous equation. The detailed process is (Winget and Hughs, 1985):

1. Initialization:

$$m = 0,$$

$$\mathbf{R}_0 = \mathbf{B} - \mathbf{SX}_0,$$

$$\mathbf{Z}_0 = \mathbf{P}_0 = \mathbf{Q}^{-1}\mathbf{R}_0.$$

2. $$\alpha = \frac{(\mathbf{R}_m, \mathbf{P}_m)}{(\mathbf{P}_m, \mathbf{SP}_m)},$$

$$\mathbf{X}_{m+1} = \mathbf{X}_m + \alpha \mathbf{P}_m,$$

$$\mathbf{R}_{m+1} = \mathbf{R}_m - \alpha \mathbf{SP}_m.$$

(3) Convergence check:

If $\|\mathbf{R}_{m+1}\| < \varepsilon \|\mathbf{B}\|$, return, Or else, continue

(4) $\mathbf{Z}_{m+1} = \mathbf{Q}^{-1}\mathbf{R}_{m+1}$,

$$\mathbf{P}_{m+1} = \mathbf{Z}_{m+1} + \frac{(\mathbf{R}_{m+1}, \mathbf{Z}_{m+1})}{(\mathbf{R}_m, \mathbf{Z}_m)} \mathbf{P}_m,$$

$$m = m + 1.$$

Wang et al. (2007) analyzed the accuracy and efficiency of the Chebyshev and the Legendre SEM.

Numerical examples

The algorithm to simulate elastic wave propagation is validated by coding a program in the Fortran language. In the following numerical examples, the source applied along the horizontal and vertical directions at point S is the particle velocity of the vibration with equal particle velocity components in the two directions. The wavelet source function is the first derivative of the Gaussian function and its central frequency is 10 Hz. The normalized waveform is plotted in Figure 2. During the calculations, a damping absorbing boundary condition is adopted to reduce the effects of the artificial boundaries (Cerjan et al., 1985).

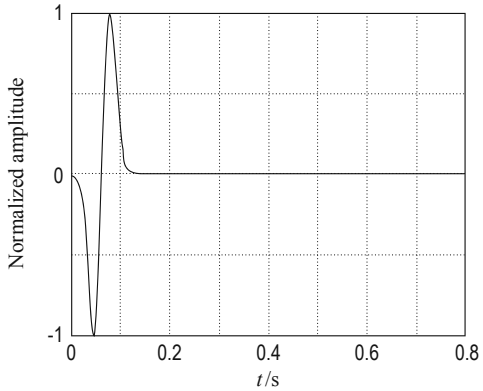

Fig. 2 Source seismogram.

Example 1 : A homogeneous medium model

In order to validate the accuracy of the proposed algorithm, a homogeneous model is chosen and shown in Figure 3.It is a square with a length of 3000 m with compressional and shear velocities and density of v_c=2900 m/s, v_s = 1674 m/s, and ρ=1900 kg/m^3. The source is applied at point S (1500m, 1500m) and the first receiver R_1 is located at (2400m, 1500m) and the second is at (1500m, 2100m).

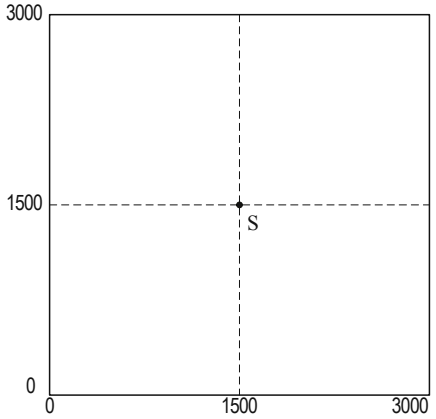

Fig. 3 The homogeneous medium model.

To demonstrate the accuracy of the SEM, the modeling results of the 8-order staggered FDM is compared with those of the SEM. More detailed work about the FDM is given in Wang (2001). In the FDM, the model is discretized into 1500 by 1500 grid meshes and the size of each mesh is 2 by 2 m. The time step Δt is 2E-4 s. For the SEM, the same model is discretized with 300 by 300 square elements with an element size of 10 by 10 m. The time step Δt is 2E-3 s. Thus, the computational area of the SEM is larger than that of the FDM. Figures 4a and 4b display the snapshots of the horizontal particle velocity component at a time of 0.5s computed by the FDM and the SEM, respectively. Figures 4c and 4d display the vertical snapshots at a time of 0.5s computed by the FDM and the SEM, respectively. From these figures, we can identify the compressional and shear waves easily. Figures 5a and 5b show the waveform comparisons for the horizontal and vertical particle velocity component components at the location R_1 computed by the FDM and the SEM methods, respectively. Figures 5c and 5d show the waveform comparisons for the horizontal and vertical particle velocity components at the location R_2 computed by the FDM and the SEM methods, respectively. The waveform is normalized in each figure. The agreements are excellent for all waveforms recorded at R_1 and R_2.

At the same time, the finite element method (FEM) is also used to compute the same model. The results show that the SEM exceeds the FEM in both computational accuracy and computational efficiency. The detailed computational results are not shown due to the limited paper space.

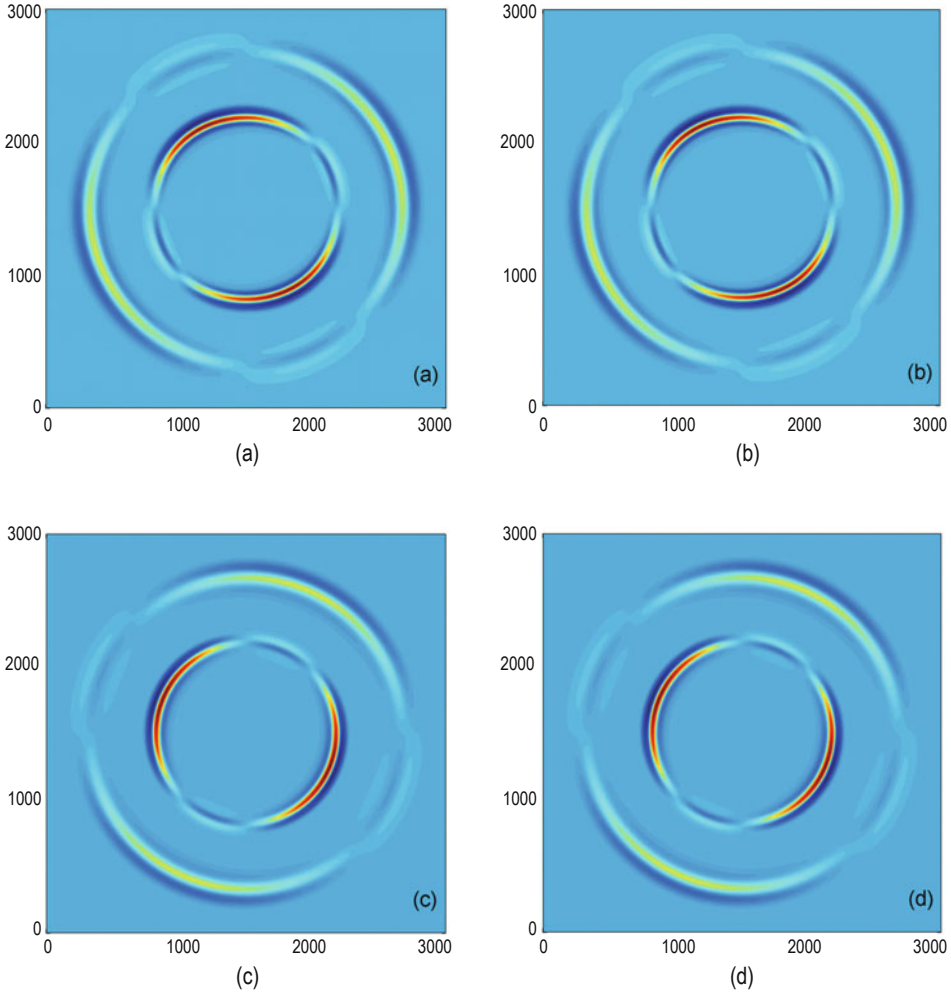

Fig. 4 Snapshot comparisons of horizontal (a and b) and vertical (c and d) velocity components at a time of 0.5s computed by the FDM (a and c) and the SEM (b and d), respectively.

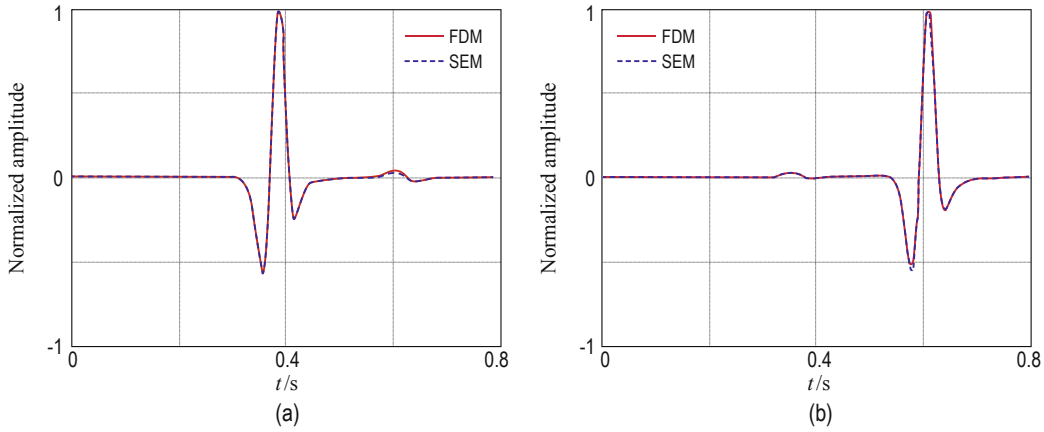

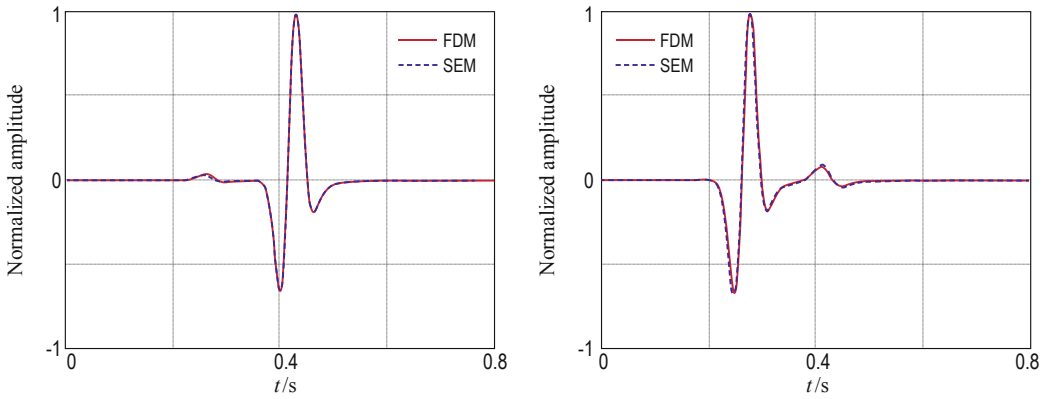

Fig. 5 Waveform comparisons for the horizontal and vertical particle velocity components at the locations R_1 (a and b) and R_2 (c and d) computed by the FDM and the SEM methods, respectively. The solid and dashed lines stand for the waveforms calculated with the FDM and the SEM methods, respectively.

Example 2: A homogeneous medium model with an inclined layer

A homogeneous medium model with an inclined layer is shown in Figure 6. The model is a square with a side length of 3000 m. It consists of two quadrilateral formations with an inclined layer whose angle is 26.6º, centered in the square. The formation above the incline is a fast one with compressional and shear velocities and density $v_c = 3600$ m/s, $v_s = 2079$ m/s, and $\rho = 2680$ kg/m^3, respectively. The formation under the incline is a slow one with the compressional and shear velocities and density $v_c = 2900$ m/s, $v_s = 1674$ m/s, and $\rho = 1900$ kg/m^3, respectively. The source is applied at point S with coordinates (1500m, 1200m) and a receiver R at (1500m, 1800m).

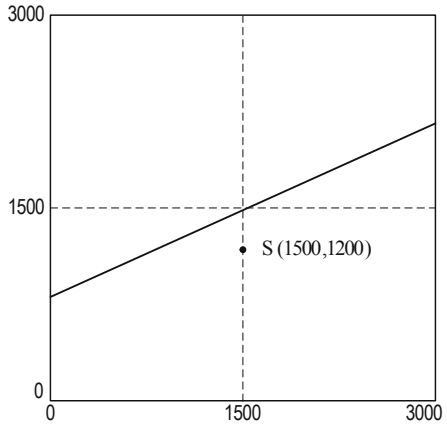

Fig. 6 The elastic model with an inclined interface.

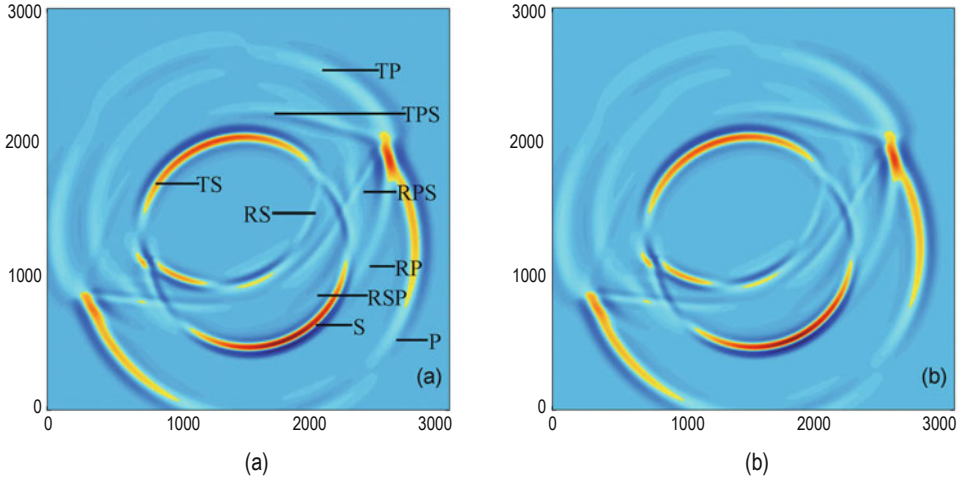

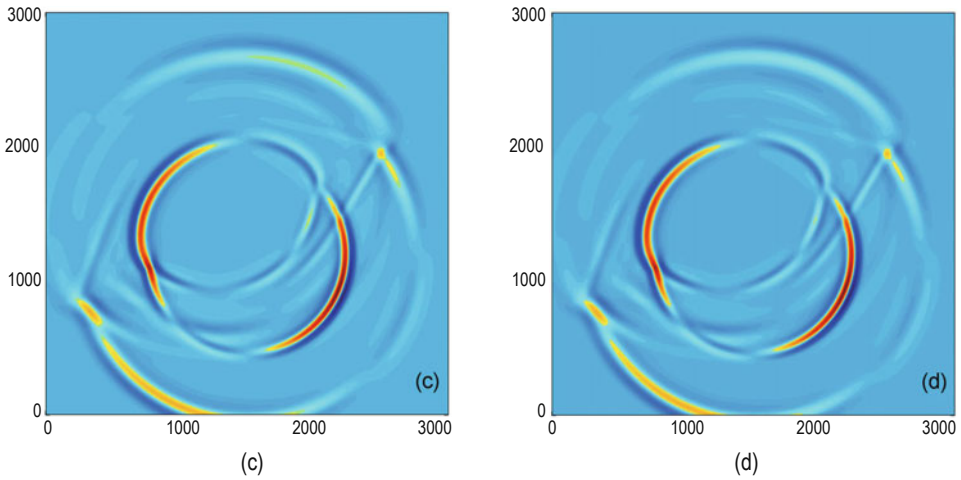

Fig. 7 Snapshot comparisons of horizontal (a and b) and vertical (c and d) particle velocity components at a time of 0.5s computed by the FDM (a and c) and the SEM (b and d), respectively.

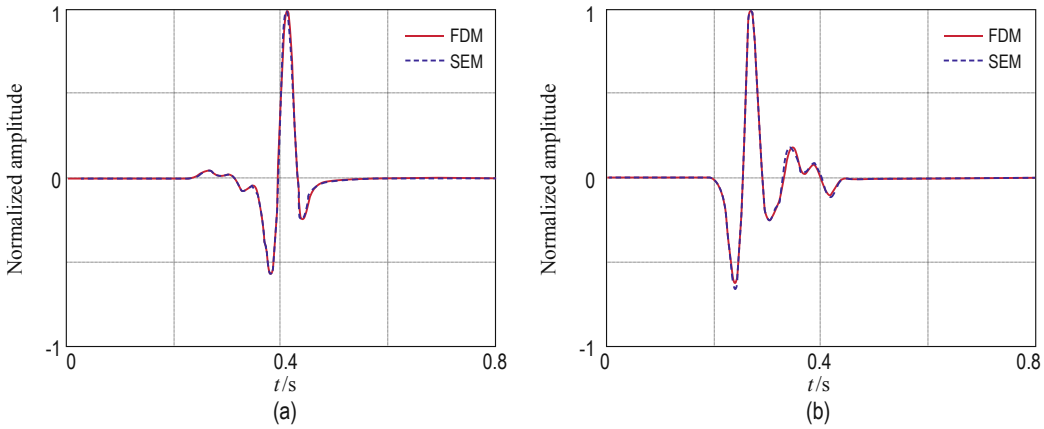

Fig. 8 Waveform comparisons for horizontal and vertical particle velocity components at the location R computed by the FDM (solid lines) and the SEM (dashed lines), respectively.

The modeling results computed by the FDM and the Chebyshev SEM are compared. In the FDM, the model is discretized into 1500 by 1500 grid mesh with the size of each mesh 2 by 2 m. The time step Δt is 2E-4 s. The SEM model is discretized with 300 by 300 quadrilateral elements but their shape no longer a square. The time step Δt is 2E-3s. Figures 7a and 7b display the horizontal particle velocity snapshots at a time of 0.5 s computed by the FDM and SEM, respectively. Figures 7c and 7d display the vertical component snapshots at a time of 0.5s computed by the FDM and the SEM, respectively. From these figures, we can identify the direct compressional wave (P), direct shear wave (S), reflected compressional wave (RP), reflected shear wave (RS), transmitted compressional wave (TP), transmitted shear wave (TS), and some converted waves (RPS, RSP, TPS) clearly. Figures 8a and 8b show the waveform comparisons for the horizontal and vertical particle velocity components at the location R computed by the FDM and the SEM methods, respectively, and the agreement is excellent.

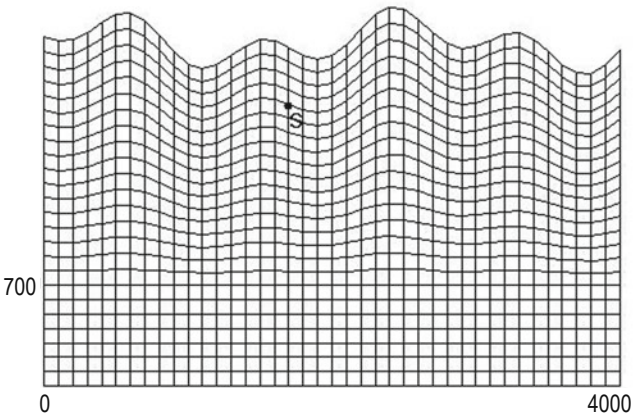

Fig. 9 The homogeneous layered model with a topographic traction free surface, and its element arrangements.

Example 3: A homogeneous medium model with a topographic traction free surface

Presently, some improved FDM and other methods can deal with the gradually varying geography while modeling wave propagation along a free boundary but the computational accuracy cannot exceed the second order (Wang and Zhang, 2004). On the other hand, the capability of handling a topographic traction free surface is one of the major advantages of the SEM, for the free boundary conditions are satisfied naturally. So now we consider a homogeneous medium model with a topographic traction free surface. Figure 9 shows a two-dimensional topographical profile with a traction free surface and its element arrangement. The width of the model is 4000 m and the maximum and minimum elevation of the free surface is 2930 m and 2470 m. The topographical surface is described by a combination of a sine function and a cosine function. A horizontal layer is 700 m above the bottom boundary. The upper formation is a slow one with compressional and shear velocities and density v_c=2900 m/s, v_s=1674 m/s, and ρ=1900 kg/m^3. The lower formation is a fast one with compressional and shear velocities and density v_c=4000 m/s, v_s=2309 m/s, and ρ=2680 kg/m^3. The source is applied at point S with coordinates (2000m, 2250m). The model is discretized with 400 by 240 quadrilateral elements. The time step Δt is 2E-3 s.

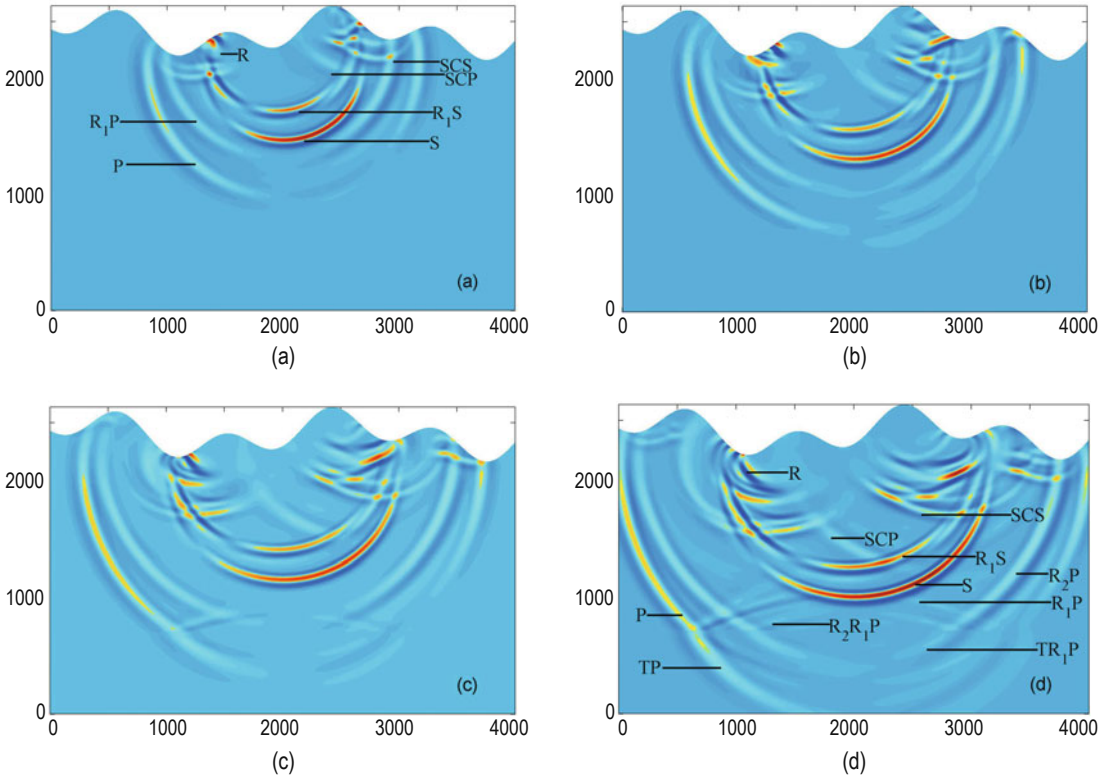

Fig. 10 Snapshots of horizontal velocity components at times 0.5s, 0.6s, 0.7s and 0.8s computed by the SEM method.

Figures 10a to 10d display the horizontal particle velocity snapshots at times of 0.5 s, 0.6 s, 0.7 s, and 0.8 s computed by the SEM method. Figures 11a and 11b display the seismograms of horizontal and vertical particle displacement components along the free surface computed by the SEM method. From the snapshots, we can identify the direct compressional wave (P), direct shear wave (S), reflected compressional wave (R_1P), and reflected shear wave (R_1S) at the free surface. We can also clearly see the reflected compressional wave (R_2P, R_2R_1P) and transmitted compressional wave (TP, TR_1P) at the horizontal layer. Besides, we also find that the rolling ground causes not only the elastic wave travel time shift but also the transformation between the body and surface waves. We observe a strong Rayleigh wave (R) following the compressional and shear waves, scattered compressional wave (SCP), and scattered shear wave (SCS). These surface and scattered waves can be confused with the reflected waves from deep, middle, and shallow layers, which results in a low signal/noise ratio. Generally, some interfering waves in real seismic recordings are caused by the uneven

ground surface and that is a major factor resulting in seismic data with low signal/noise ratio in mountainous areas. We can identify various superficial interfering waves by modeling the propagation of elastic waves which can be used to guide the process of denoising in real seismic data.

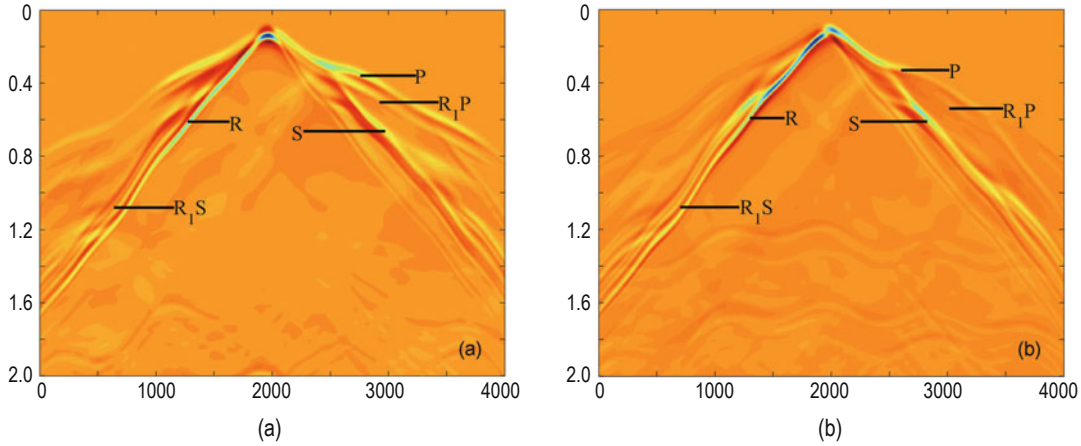

Fig. 11 Horizontal (a) and vertical (b) displacement seismograms along the free surface computed by the SEM method.

Conclusions

In this paper, based on the Galerkin variational principle constructed with Chebyshev orthogonal polynomials, we propose an improved spectral element method by introducing the preconditioned conjugate gradient (PCG) element by element (EBE) algorithm in the spatial domain and the staggered predictor/corrector algorithm in the time domain. Trial calculations are performed on several models. The modeling results of the SEM are compared to FDM for a homogeneous medium and a medium with an inclined interface and the results are in good agreement. The numerical results show that the Chebyshev SEM can get the equivalent accuracy with the FDM by using fewer mesh grid nodes and a longer time iteration step. The SEM is also used to simulate the wave propagation in a layered medium with a topographic traction free surface and the evolutionary process of wavefield snapshots and various waveform components are obtained clearly. Since the SEM keeps the advantage of handling random geography and free boundaries of the FEM, it is available for modeling elastic wave propagation in complex formations with irregular free surfaces.

References

Alford, R. M., Kelly, K. R., and Boore, D. M., 1974, Accuracy of finite difference modeling of the acoustic wave equation: Geophysics, **39**(6), 834 – 842.

Alterman, Z. S., and Loewenthal, D., 1970, Seismic waves in a quarter and three-quarter plane: Geophys. J. Roy. Astr. Soc., **20**(2), 101 – 126.

Canuto, C., Hussaini, M. Y., Quarteroni, A., and Zang, T. A., 1988, Spectral methods in fluid dynamics: Springer-Verlag, 65 – 75.

Cerjan, C., Kosloff, D., Kosloff, R., and Reshef, M., 1985, A non-reflecting boundary condition for discrete acoustic and elastic wave equations: Geophysics, **50**(4), 705 – 708.

Deng, S. Z., Zhou, S. Q., and Zeng, L., 1995, Application of EBE strategy in structural analysis (I)-EBE computational method for matrix-vector multiply and its parallel/vector implementations: Journal of Astronautics, **16**(2), 13-19.

Gazdag, J., 1981, Modeling of the acoustic wave equation with transform method: Geophysics, **46**(6), 854 – 859.

Hilber, H. M., Hughes, T. J. R., and Taylor, R. L., 1977, Improved numerical dissipation for time integration algorithms in structural dynamics: Earthquake Engineering and Structural Dynamics, **5**, 283 – 292.

Hughes, T. J. R., 1987, The finite element method — Linear static and dynamic finite element analysis: Prentice-Hall, Inc, Englewood Cliffs, New Jersey.

Hughes, T. J. R., Levit, I., and Winget, J., 1983a, Element-by-element implicit algorithms for heat conduction: Journal of Engineering Mechanics, **109**(2), 576 – 585.

Hughes, T. J. R., Levit, I., and Winget, J., 1983b, An element-by-element solution algorithm for problems of structural and solid mechanics: Computer Methods in

Applied Mechanics and Engineering, **36**(2), 241 – 254.
Komatitsch, D., and Barnes, C., 2002, Spectral-element simulations of global seismic wave propagation—II. Three-dimensional models, oceans, rotation and self-gravitation: Geophys. J. Int., **150**, 303 – 318.
Komatitsch, D., Barnes, C., and Tromp. J., 2000a, Wave propagation near a fluid-solid interface: A spectral-element approach: Geophysics, **65**(2), 623 – 631.
Komatitsch, D., Barnes, C., and Tromp. J., 2000b, Simulation of isotropic wave propagation based upon a spectral element method: Geophysics, **65**(4), 1251 – 1260.
Komatitsch, D., Barnes, C., and Tromp. J., 2002, Spectral-element simulations of global seismic wave propagation-I. Validation: Geophys. J. Int., **149**, 390 – 412.
Komatitsch, D., and Vilotte, J. P., 1998, The spectral element method: an efficient tool to simulate the seismic response of 2-D and 3-D geological structures: Bull. Seis. Soc. Am., **88**(2), 368 – 392.
Komatitsch, D., Vilotte, J. P., Vai, R., Castillo-Covarrubias, J. M., and Sanchez-Sesma, F. J., 1999, The spectral element method for elastic wave equations-application to 2-D and 3-D seismic problems: Int. J. Meth. Eng., **45**, 1139 – 1164.
Kosloff, D., and Baysal, E., 1982, Forward modeling by a Fourier method: Geophysics, **47**(10), 1402 – 1412.
Kosloff, D., Kessler, D., Filho, A. Q., Behle, A., and Strabilevitz, R., 1990, Solution of the equations of dynamic elasticity by a Chebyshev spectral method: Geophysics, **55**(6), 734 – 748.
Lin, W. J., Wang, X. M., and Zhang, H. L., 2006, An element by element spectral element method for elastic wave modeling: Progress in Natural Science, **16**(1), 21 – 29.
Patera, A. T., 1984, A spectral element method for fluid dynamics: laminar flow in a channel expansion: Journal of Computational Physics, **54**(3), 468 – 488.
Seriani, G., 1997, A parallel spectral element method for acoustic wave modeling: J. Computation Acoustics, **5**(1), 53 – 69.
Seriani, G., 1998, 3-D large-scale wave propagation modeling by spectral element method on Cray T3E: Comp. Meth. Appl. Mech. and Eng., **164**, 235 – 247.
Seriani, G., and Priolo, E., 1994, Spectral element method for acoustic wave simulation in heterogeneous media: Finite element in analysis and design, **16**, 337 – 348.
Seriani, G., Priolo, E., Carcione, J. M., and Padovani, E., 1992, High-order spectral element method for elastic wave modeling: 62th Ann. Internat. Mtg., Soc. Expl. Geophys., Expanded Abstracts, 1285 – 1288.
Wang, X. M., 2001, Seismic wave simulation in anisotropic media with heterogeneity using high-order finite-difference method: In Proceedings of the 5th SEGJ International Symposium: Imaging Technology, Tokyo, Japan, 113 – 120.
Wang, X. M., Dodds, K., and Zhao, H. B., 2006, An improved high-order rotated staggered finite-difference algorithm for simulating elastic waves in heterogeneous viscoelastic/anisotropic media: Exploration Geophysics, **37**(2), 160 – 174.
Wang, X. M., Seriani, G., and Lin, W. J., 2007, Some theoretical aspects of elastic wave modeling with a recently developed spectral element method: Science in China (Series G), **50** (2), 185 – 207.
Wang, X. M., and Zhang, H. L., 2004, Modeling of elastic wave propagation on a curved free surface using an improved finite-difference algorithm: Science in China (Series G), **47** (5), 633 – 648.
Winget, J., and Hughes, T. J. R., 1985, Solution algorithms for nonlinear transient heat conduction analysis employing element-by-element iterative strategies: Computer Methods in Applied Mechanics and Engineering, **52**, 711 – 815.

Che Chengxuan received his master degree in Geodetection and Information Technology from Northeast Petroleum University in 2007. He is currently a PhD student majoring in reservoir acoustic characterizations and borehole exploration in Institute of Acoustics, Chinese Academy of Sciences. His research interests include numerical simulation of seismic waves, numerical simulation and experimental measurement of production well-logging.